

Article

Tribo-oxide Competition and Oxide Layer Formation of Ti_3SiC_2/CaF_2 Self-Lubricating Composites during the Friction Process in a Wide Temperature Range

Rui Zhang ^{1,2,3,4,*}, Wei Feng ^{1,2} and Fuyan Liu ⁵

¹ School of Mechanical Engineering, Chengdu University, Chengdu 610106, China; fengwei@cdu.edu.cn

² Sichuan Province Engineering Technology Research Center of Powder Metallurgy, Chengdu University, Chengdu 610106, China

³ Institute for Advanced Materials Deformation and Damage from Multi-Scale, Chengdu University, Chengdu 610106, China

⁴ School of Mechanical Engineering, Xinjiang University, Urumqi 830000, China

⁵ School of Chemical Engineering and Materials, Changzhou Institute of Technology, Changzhou 213032, China; liufy@czu.cn

* Correspondence: zhangrui0214@cdu.edu.cn



Citation: Zhang, R.; Feng, W.; Liu, F. Tribo-oxide Competition and Oxide Layer Formation of Ti_3SiC_2/CaF_2 Self-Lubricating Composites during the Friction Process in a Wide Temperature Range. *Materials* **2021**, *14*, 7466. <https://doi.org/10.3390/ma14237466>

Academic Editor: Emanuela Cerri

Received: 9 November 2021

Accepted: 30 November 2021

Published: 6 December 2021

Publisher's Note: MDPI stays neutral with regard to jurisdictional claims in published maps and institutional affiliations.



Copyright: © 2021 by the authors. Licensee MDPI, Basel, Switzerland. This article is an open access article distributed under the terms and conditions of the Creative Commons Attribution (CC BY) license (<https://creativecommons.org/licenses/by/4.0/>).

1. Introduction

MAX phase ceramics have received widespread attention owing to their having properties of both ceramics and metals [1,2]. The term “ $M_{n+1}AX_n$ phase” was first used by Barsoum [2]. The general formula $M_{n+1}AX_n$ was abbreviated to MAX. The Ti_3SiC_2 ceramic was one of the representative MAX ceramic materials [3–7]. Although it showed the duality of tribology, its self-lubricating properties were not obvious [8–10]. Related research found that doping the hard phase or lubricating phase to improve the tribological properties of Ti_3SiC_2 was effective [11–17]. However, like solid lubricants of graphite or MoS_2 , it can be severely oxidized in a high-temperature atmosphere, restricting its use in lubrication above 500 °C [18].

Fluoride had high melting point, good chemical stability and thermal stability. It is still very stable in both high-temperature, extremely oxidative atmospheres, and high-temperature, extremely reducing atmospheres [19–21], and it is not easy to oxidize and decompose. Moreover, it softens and forms ductile phases at high temperatures [22]. In the research of high-temperature-tolerant self-lubricating composite materials, fluoride has always been the first choice for solid lubricants. After fluorides undergo the transition from toughness to brittleness, they can form a stable separating film with low shear on the friction surface, allowing them to effectively exert their lubricating properties in the working environment [23–25]. Among them, CaF_2 is a high-temperature solid lubricant

with excellent performances. It had good chemical stability at 25–1000 °C. Additionally, it shows good high temperature lubrication performance due to the change from brittleness to plasticity during mechanical friction at above 500 °C. It is thought that the good friction and wear performance of this material is mainly owed to CaF₂ forming a solid lubricating film on the surface in a high temperature environment.

In this paper, by using CaF₂ as a solid lubricant, a Ti₃SiC₂-based self-lubricating composite (abbreviated as TSC-CF) was synthesized via SPS process. The effect of CaF₂ on the structure of TSC-CF was investigated, and its friction and wear properties at 25–800 °C were explored.

2. Experiment

2.1. Preparation of Samples

All of the samples were prepared by SPS (Shanghai Chenhua Electric Furnace Co., Ltd., Shanghai, China). The composites were fabricated using powders of Ti₃SiC₂ (Jinhezhi Materials Ltd., Beijing, China) and CaF₂ (Xinshengshi Chemical Technology Co., Ltd., Shanghai, China). The purity of the powder directly affected the performance of the prepared samples, so Ti₃SiC₂ powder with a purity of 98% and CaF₂ powder with a purity of 98.5% were used for sample preparation. For the particle size, the sample sintered with fine-grained Ti₃SiC₂ powder had smaller grains and had better mechanical properties and wear resistance. Therefore, Ti₃SiC₂ powder with a particle size of 3 μm was selected. Additionally, CaF₂ powder with overly small particles is not conducive to uniform powder mixing, so the CaF₂ powder with a particle size of 74 μm was chosen. The volume fraction of CaF₂ in Ti₃SiC₂-CaF₂ composite powder was 15.

The Ti₃SiC₂-CaF₂ composite powder was sintered at 1200, 1250, 1300 and 1350 °C, respectively. The heating rate and pressure were 50 °C/min and 35 MPa. The holding time was 5 min at maximum temperature, and then cooling to 1000 °C, followed by holding at 1000 °C for 15 min. For the purpose of comparison, pure Ti₃SiC₂ bulk materials (abbreviated as TSC) were sintered under the same conditions.

2.2. Mechanical Properties

The relative density of the composite material was determined by using Archimedes' principle [26]. Micro-hardness was measured by a MH-5-VM Micro-hardness Tester (Shanghai Hengyi Technology Co., Ltd., Shanghai, China). A load of 4.9 N and a dwell time of 10 s were used. Flexural strength and compression strength were measured with a SANS-CMT5205 universal material tester (Shenzhen New Sansi Material Testing Co., Ltd., Shenzhen, China). The flexural strength and compression strength were measured with a universal testing machine. the samples sizes for flexural strength and compression strength were 3 mm high × 4 mm wide × 20 mm long and Φ 5 mm × 12.5 mm, respectively.

2.3. Friction and Wear Test

The friction and wear experiments used a pin-on-disk configuration (THT01-04015, CSM Instruments SA, Peseux, Switzerland). The pin was made of Ti₃SiC₂ and Ti₃SiC₂/CaF₂ sample with a size of Φ6 mm × 12 mm. The disk was made of Inconel 718 alloys with a size of Φ32 mm × 8 mm. The sliding velocity, normal load and sliding distance were 0.1 m/s, 5 N and 200 mm, respectively. The friction coefficient was automatically collected during the experiment. The volume loss method was used to calculate the wear volume. The cross-sectional area of the wear track on Inconel 718 disk was measured using optical microscopy and the dual-mode three-dimensional surface profiler (NanoMap-D, Columbus, OH, USA).

2.4. Analysis

The morphologies of worn surfaces were observed by a JSM-5600LV scanning electron microscopy (SEM, JEOL, Tokyo, Japan) which was equipped with energy dispersive spectroscopy (EDS). The X-ray photoelectron spectroscope (XPS, PHI-5702, Physical Electronics

Corporation, Chanhassen, MN, USA) was used for the determined of elements chemical states on the worn surfaces.

3. Results

3.1. Phase Composition and Microstructure

The XRD results (Figure 1) showed that the composites (85 vol.% Ti_3SiC_2 -15 vol.% CaF_2) sintered at 1200 and 1250 °C were mainly composed of Ti_3SiC_2 and CaF_2 , indicating that no reactions occurred between them and that Ti_3SiC_2 did not decompose. At 1300 °C, besides Ti_3SiC_2 and CaF_2 , diffraction peaks of $\text{Ti}_5\text{Si}_3\text{C}_x$ were detected. This new phase was guessed to form due to the escapement of Si atoms from the crystal lattice of Ti_3SiC_2 . The Si atoms moved along the base plane of the Ti_3SiC_2 crystal and then left the grain boundary at high temperatures [2]. After the escapement of Si atoms, the Ti_3C_2 framework was left, forming TiC_x because of the relaxation of Ti_3C_2 and the rearrangement of C atoms ($\text{Ti}_3\text{SiC}_2 \rightarrow \text{Si} + \text{Ti}_3\text{C}_2(\text{TiC}_x)$). On the other hand, Si atoms reacted with Ti_3C_2 nearby to form $\text{Ti}_5\text{Si}_3\text{C}_x$ ($\text{Ti}_3\text{C}_2(\text{TiC}_x) + \text{Si} \rightarrow \text{Ti}_5\text{Si}_3\text{C}_x$). Finally, Si atoms combined with Ti_3SiC_2 to form $\text{Ti}_5\text{Si}_3\text{C}_x$ ($\text{Ti}_3\text{SiC}_2 + \text{Si} \rightarrow \text{Ti}_5\text{Si}_3\text{C}_x$) [27]. Therefore, $\text{Ti}_5\text{Si}_3\text{C}_x$ existed in the TSC-CF composite mainly due to the incomplete decomposition of Ti_3SiC_2 . In comparison with our previous study, the addition of CaF_2 promoted the decrease in decomposition temperature of Ti_3SiC_2 from 1350 to 1300 °C. SEM results indicated the grains of Ti_3SiC_2 in TSC-CF composites were granular. Additionally, compared with the original Ti_3SiC_2 powder, the grains of Ti_3SiC_2 in the TSC-CF composite were obviously larger, and their size increased with the sintering temperature.

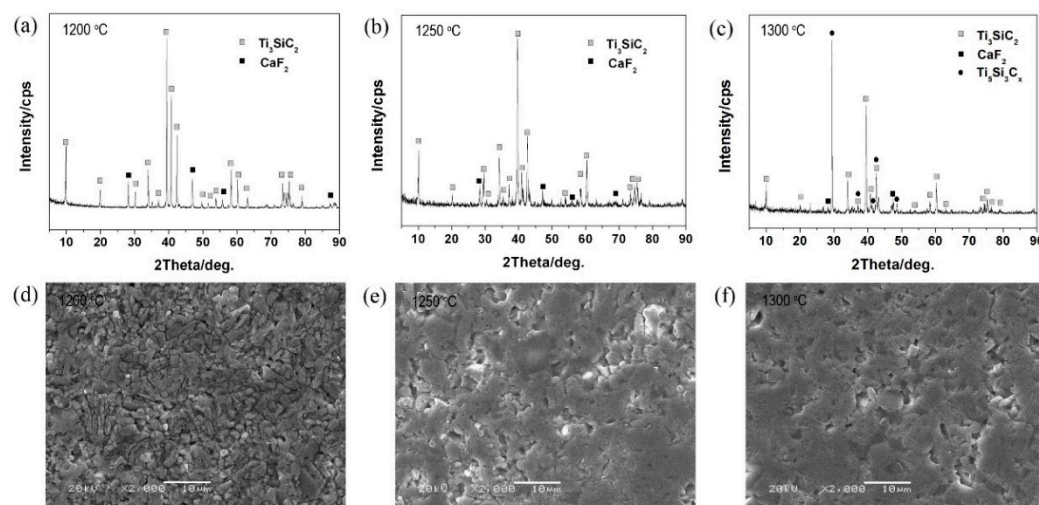


Figure 1. XRD pattern and SEM images of TSC-CF composites.

3.2. Mechanical Properties

As temperature increased, the relative density and bending strength of TSC did not change significantly, which were about 98.24% and 422.67 ± 6.8 MPa, respectively. As the sintering temperature of TSC increased, its hardness increased from 5 to 5.8 GPa, and its compressive strength rose from 1100 to 1234 MPa. As for the TSC-CF composite, both relative density and compressive strength increased with the sintering temperature. Additionally, the bending strength and hardness of TSC-CF composites were insensitive to the sintering temperature, and remained at 4.9 ± 0.1 GPa and 312.3 ± 3.79 MPa, respectively. In comparison, the relative density, hardness, compressive strength and flexural strength of the TSC-CF composite were lower than those of TSC, due to the addition of CaF_2 . It is shown in Figure 2 that both TSC and TSC-CF composites had better mechanical properties at 1250 °C.

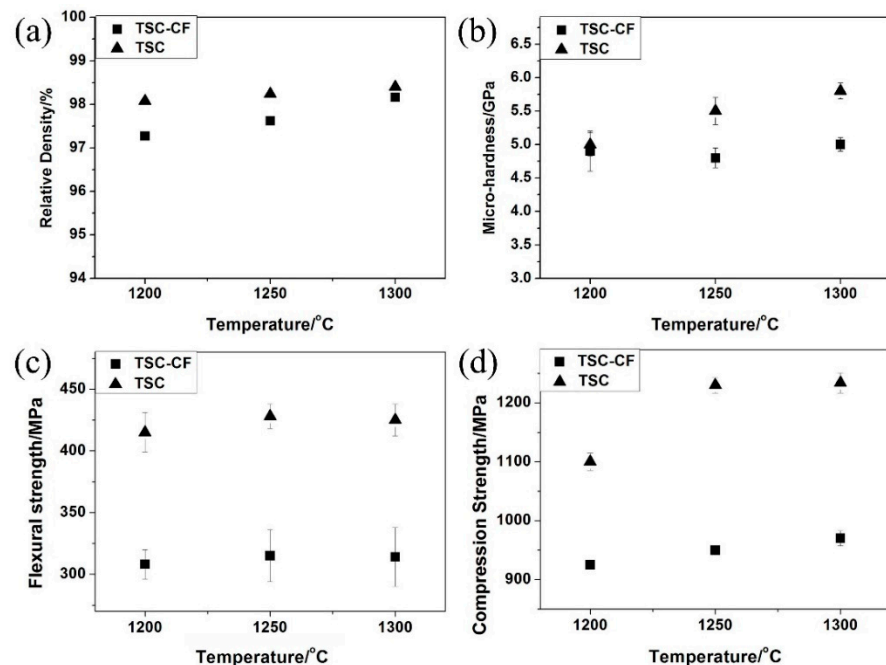


Figure 2. The (a) relative density, (b) micro-hardness, (c) flexural strength and (d) compression strength of TSC and TSC-CF at different temperatures.

As seen in Figure 3a, TSC-CF composites only underwent elastic deformation before fracture, similarly to TSC. It was deduced that the addition of CaF_2 did not change the fracture mode of Ti_3SiC_2 . Additionally, the brittle fracture behavior at room temperature was also found in the bending fracture morphology of the TSC-CF composites (see Figure 3b–d), and a large number of Ti_3SiC_2 grains were distributed in a disordered manner, which was visible from a macroscopic view.

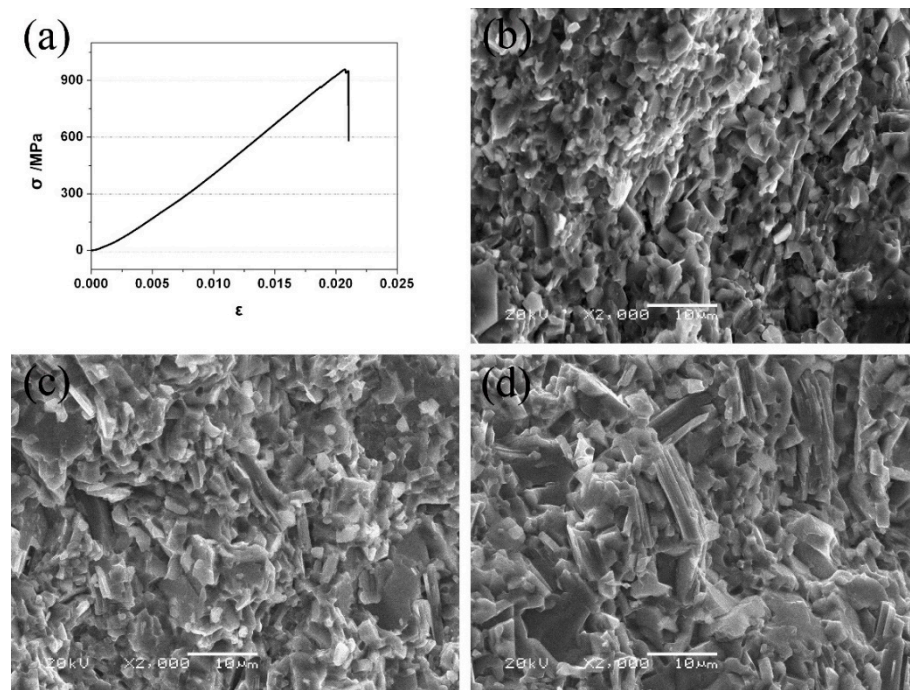


Figure 3. (a) Compressive stress–strain curve of the TSC-CF composite exposed to different sintering temperatures, and cross-sectional maps after the three-point bending test: (b) 1200 °C, (c) 1250 °C and (d) 1300 °C.

3.3. Friction Coefficients and Wear Rates

Both TSC and TSC-CF sintered at 1250 °C had better mechanical properties, so their friction and wear properties against Inconel 718 alloy at 25–800 °C were investigated for comparison purposes.

The relationship between the friction coefficients of TSC/Inconel 718 and TSC-CF/Inconel 718 pairs with sliding distance and their average friction coefficients at different friction test temperatures are shown in Figure 4. The friction coefficient of the TSC/Inconel 718 alloy pair had a large fluctuation at 25–200 °C and was relatively stable above 400 °C. However, the friction coefficient of the TSC-CF/Inconel 718 alloys pair greatly fluctuated at 25–600 °C and kept stable after 800 °C. TSC/Inconel 718 had no obvious running-in period during the friction process. TSC-CF/Inconel 718 had an obvious running-in period at 800 °C. As the sliding temperature increased from 25 to 800 °C, the average friction coefficient of the TSC-CF/Inconel 718 alloys pair showed a downward trend (from 0.81 to 0.34). In comparison, the average friction coefficient of TSC-CF was higher than that of TSC at 25–400 °C, and it was lower than that of TSC at above 600 °C, owing to the addition of CaF₂. In other words, CaF₂ played had a certain self-lubricating effect above 600 °C.

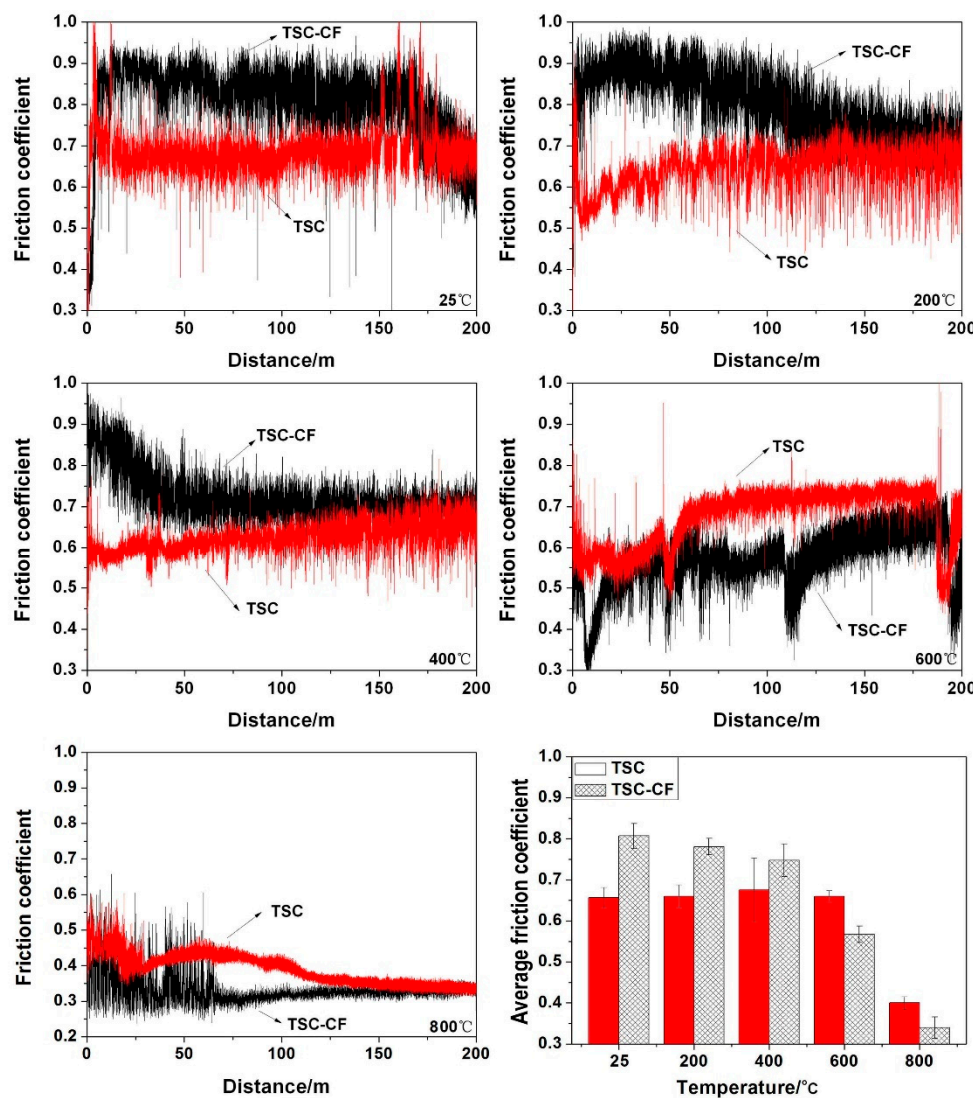


Figure 4. The friction coefficients of the TSC and TSC-CF with different temperature.

As shown in Figure 5, the wear rate of the TSC pin in the TSC/Inconel 718 pair gradually decreased to $10^{-6} \text{ mm}^3/\text{Nm}$ from 25 to 800 °C. The wear rate of the TSC-CF

pin in the TSC-CF/Inconel 718 pair was insensitive to the temperature (25–800 °C) and remained at 10^{-3} mm³/Nm. In comparison, the wear rate of the TSC-CF pin was greater than that of TSC at 25–800 °C. The wear resistance of the TSC-CF composite was lower than that of TSC, which might have resulted from the lower hardness of the TSC-CF composite (see Figure 4). As we all know, the wear resistance of a material largely depends on the hardness of the material. When sliding against TSC, the wear rate of the disc gradually decreased as the temperature increased from 25 to 600 °C, and remained at a magnitude of 10^{-5} mm³/Nm. However, negative wear occurred at 800 °C for the Inconel 718 alloy disc in the TSC/Inconel 718 pair. When grinding with TSC-CF, the wear rate of the Inconel 718 disc was similar to that of TSC.

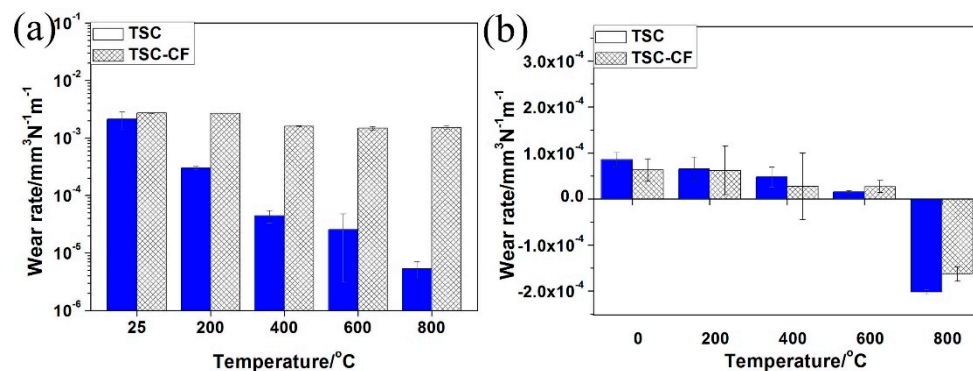


Figure 5. The wear rates of the (a) pin and (b) disk of the TSC/Inconel 718 and TSC-CF/Inconel 718 alloy tribo-pair.

In short, though the wear resistance of TSC-CF composites was worse than that of TSC at 25–800 °C, the TSC-CF composites exhibited better self-lubricating properties than TSC at 600–800 °C. Therefore, CaF₂ was effective for using Ti₃SiC₂ as a solid lubricant at 600–800 °C.

3.4. Morphologies and Compositions of Worn Surfaces

The wear morphology of the pin and disc in the TSC-CF/Inconel 718 pair at 25–800 °C is shown in Figure 6. It shows that the wear surface of the TSC-CF composite was similar to that of Ti₃SiC₂. At 25–400 °C, many pits were seen on the wear surface of TSC-CF composite, which were caused by the pulling out and shedding of Ti₃SiC₂ grains (see Figure 6a–c) during sliding, making its wear surface relatively rough. The Ti and Si elements from the TSC-CF composite (see d, e, f in Table 1) were found on the Inconel 718 alloy's surface (see Figure 6d–f) at 25–400 °C, indicating that one-way transfer of materials happened from the TSC-CF composite to the Inconel 718 alloy. The pulling out of the crystal grains and the shedding of the mechanical mixed layer contributed to the abrasive wear for TSC-CF/Inconel 718 pair at 25–400 °C.

As shown in Figure 6g, a plastic flow characteristic, similar to those of metal materials, was detected on the TSC-CF composite's surface at 600 °C. However, the one-way transfer of materials from the TSC-CF composite to the Inconel 718 alloy still existed for the Inconel 718 alloy disc at 600 °C. Therefore, mechanical wear on the TSC-CF composite's surface still occurred at 600 °C. At 800 °C, the plastic flow of the TSC-CF composite was more obvious, and its surface was very smooth. Additionally, there was the one-way transfer of material from TSC-CF to the Inconel 718 alloy.

The XPS analysis of Ti2p, Si2p, Ca2p and C1s on the TSC-CF's wear scar surface in the TSC-CF/Inconel 718 alloy pairs at 25–800 °C is shown in Figure 7. At 25 °C, Ti existed in Ti₃SiC₂ and TiO₂ on the worn surface of TSC-CF, and Si and Ca existed in Ti₃SiC₂ and CaO, respectively. At 600 °C and 800 °C, TiO₂, SiO₂ and CaO existed on the surface of the friction layer of TSC-CF. It was deduced that friction oxidation reactions occurred on the friction surface of TSC-CF during the sliding.

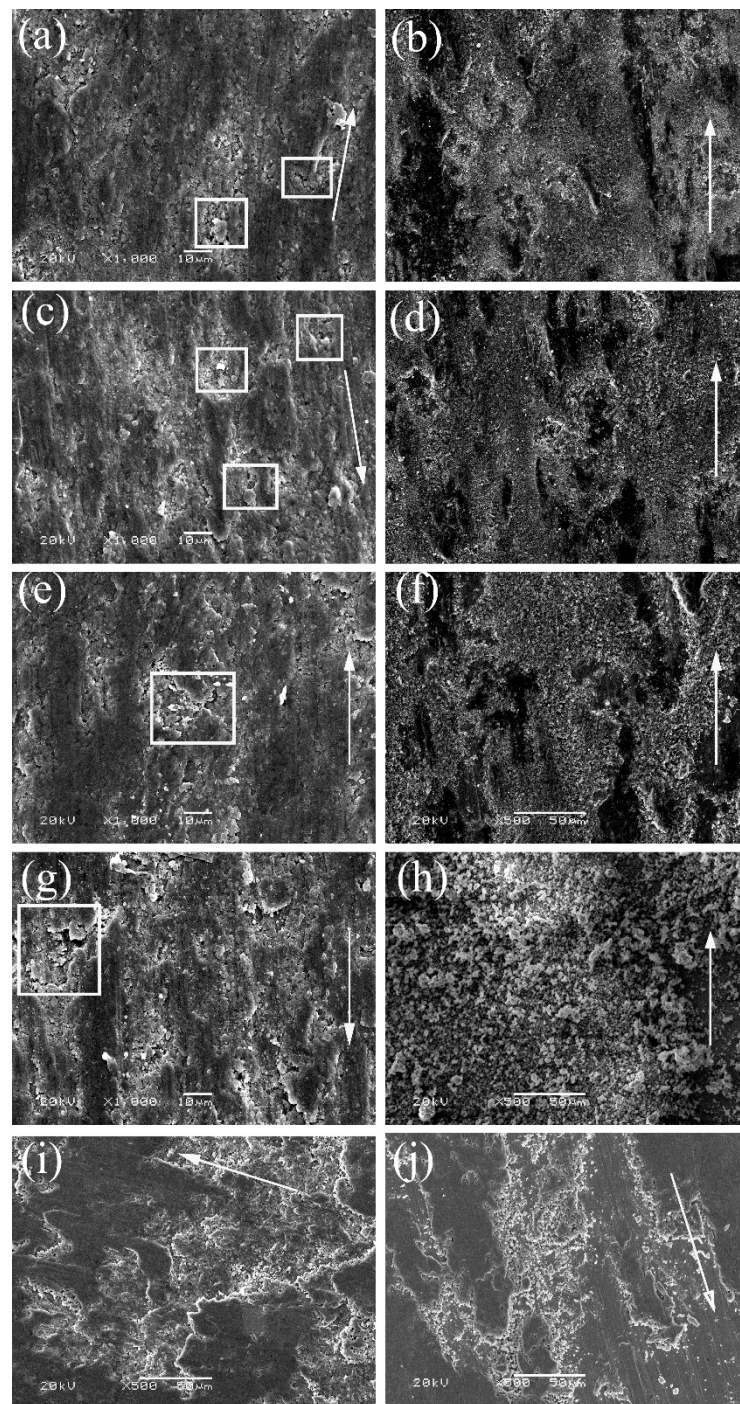
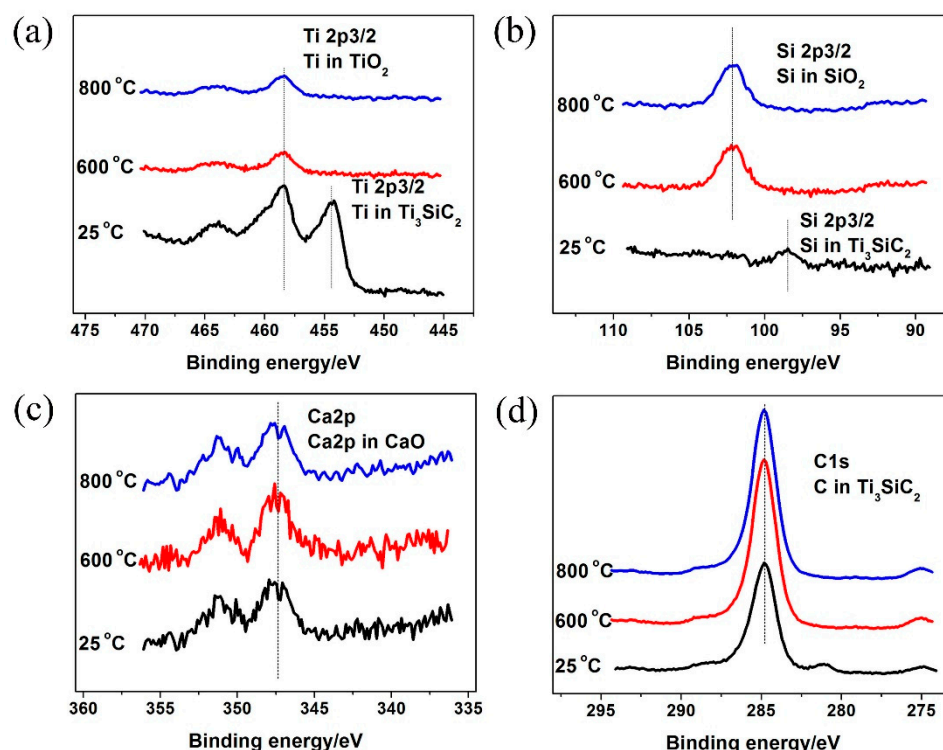


Figure 6. Worn surface of TSC-CF /Inconel 718 alloy tribo-pair: (a) TSC-CF at 25 °C, (b) Inconel 718 alloy at 25 °C, (c) TSC-CF at 200 °C, (d) Inconel 718 alloy at 200 °C, (e) TSC-CF at 400 °C, (f) Inconel 718 alloy at 400 °C, (g) TSC-CF at 600 °C, (h) Inconel 718 alloy at 600 °C, (i) TSC-CF at 800 °C, (j) Inconel 718 alloy at 800 °C.

Table 1. Atomic percentages in Figure 6.

Position	Sample	Temperature/°C	Atomic Percentages
a	TSC-CF pin	25	30.7%Ti, 13.2%Si, 41.3%C, 3.4%Al, 4.1%Ca, 7.3%F
c	TSC-CF pin	200	27.0%Ti, 11.2%Si, 44.1%C, 3.3%Al, 4.6%Ca, 9.8%F
e	TSC-CF pin	400	27.4%Ti, 10.1%Si, 47.0%C, 3.0%Al, 4.3%Ca, 8.2%F
g	TSC-CF pin	600	32.3%Ti, 9.5%Si, 42.9%C, 2.5%Al, 3.4%Ca, 9.4%F
i	TSC-CF pin	800	34.3%Ti, 8.9%Si, 41.3%C, 3.3%Al, 4.1%Ca, 8.1%F
b	Inconel 718 disk	25	15.6%Ti, 7.0%Si, 33.8%C, 1.6%Al, 2.0%Ca, 20.2%O, 9.3%F, 5.3%Ni, 2.7%Cr, 2.5%Fe
d	Inconel 718 disk	200	16.7%Ti, 7.1%Si, 32.8%C, 1.8%Al, 2.0%Ca, 23.1%O, 8.8%F, 3.8%Ni, 2.1%Cr, 1.8%Fe
f	Inconel 718 disk	400	13.7%Ti, 6.1%Si, 30.6%C, 2.0%Al, 1.6%Ca, 26.8%O, 7.6%F, 6.1%Ni, 3.0%Cr, 2.5%Fe
h	Inconel 718 disk	600	14.3%Ti, 5.2%Si, 12.7%C, 1.7%Al, 1.6%Ca, 59.8%O, 3.4%F, 0.7%Ni, 0.6%Fe
j	Inconel 718 disk	800	15.3%Ti, 5.8%Si, 11.2%C, 1.7%Al, 1.6%Ca, 59.6%O, 3.3%F, 0.9%Ni, 0.6%Fe

**Figure 7.** XPS for (a) Ti2p, (b) Si2p, (c) Ca2p and (d) C1s on the worn surface of TSC-CF at different temperatures.

4. Discussion

4.1. The Temperature's Effects on the Tribological Properties of $\text{Ti}_3\text{SiC}_2/\text{CaF}_2$

The temperature affected the friction coefficient and wear rate of TSC-CF composites. As temperature increased (25–800 °C), the friction coefficient of TSC-CF decreased. Additionally, the tribo-chemical reaction (mainly the oxidation of Ti, Si and Ca) in the friction process was a key factor affecting the tribological performance of TSC-CF composites. At 25 °C, Ti existed in the forms of Ti_3SiC_2 and TiO_2 , due to incomplete oxidation. Simultaneously, Ca was oxidized to CaO , and Si did not oxidize at 25 °C, on the friction surface of TSC-CF. The oxide generation rate was less than its consumption rate, so the oxide layer could not be formed. At above 600 °C, the formation of an oxide layer benefited from the increase in temperature, preventing direct contact between the TSC-CF composite and Inconel 718 alloy and reducing the shedding of Ti_3SiC_2 grains and material transfer. Furthermore, the oxide layers formed at elevated temperatures exhibited more obvious

plastic flow and less brittle fracturing, and were easier to shear, thereby contributing to the low friction of the TSC-CF composite at 600 and 800 °C.

4.2. Competition of Triboro-oxides

Three kinds of oxides (namely, Ti, Si and Ca oxides) on the TSC-CF composite's worn surface were detected. At 25 °C, only TiO_2 and CaO were found on the worn surface of TSC-CF, and the content of CaO was relatively greater than that of TiO_2 . At 600 °C, an oxide film consisting of TiO_2 , SiO_2 and CaO was examined on the wear surface of TSC-CF (see Figure 8). The transformation of these oxide species was due to the friction oxidation during the friction process, which in turn affected the friction and wear performance of the TSC-CF/Inconel 718 pair.

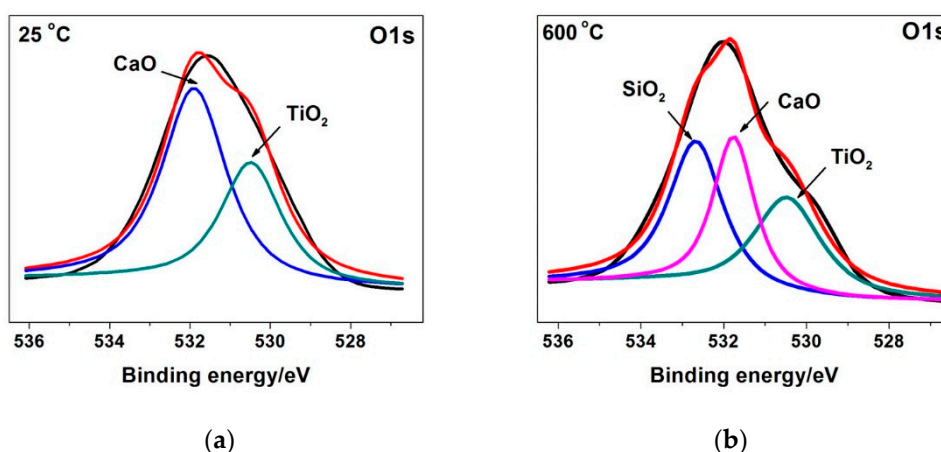


Figure 8. XPS spectra of O1s of $\text{Ti}_3\text{SiC}_2/\text{CaF}_2$ pin surface at (a) 25 °C and (b) 600 °C.

4.3. Formation of Oxide Layer

When two surfaces are sliding against each other, the work due to friction is converted into heat, causing an increase in temperature at the sliding interface. Then, the elevated temperature changes the mechanical properties of the friction surfaces, causing oxidation or even melting, all of which can cause changes in the friction coefficient and wear rate. Huang Z Y et al. [28]. pointed out that the oxidation reaction occurring on the surface of Ti_3SiC_2 originates from frictional heat, and the generation and consumption (due to wear) of the oxides occurred on the friction surface. If the generation rate was greater than the consumption rate, an oxide layer was formed. However, when the generation rate was less than the consumption rate, an oxide layer was formed or the formed oxide layer was destroyed. In fact, the test temperature for the friction experiment was also a positive factor for affecting the formation of oxides. The higher the temperature, the more favorable the formation of oxides.

At 25 °C, incomplete tribo-chemical reactions occurred on the TSC-CF composite's worn surface, only generating TiO_2 and CaO . However, the frictional heat at 25 °C was not enough to provide enough energy to promote continuous oxidation. Therefore, the oxide generation rate was lower than the consumption rate, and could not result in an oxide layer on the TSC-CF composite's surface due to the friction-reducing and anti-wear effects at 25 °C. In addition, the TSC-CF composite did not show plastic flow on its sliding surface, so the tribology properties of the TSC-CF composite at 25 °C were not improved. Compared with Ti_3SiC_2 , the oxide particles generated on the TSC-CF composite's worn surface could not form an oxide layer, and they easily fell off from the wear surface during sliding, causing more severe abrasive wear than Ti_3SiC_2 . Thus, the friction and wear of TSC-CF composite were higher than those of Ti_3SiC_2 . Above 600 °C, the TSC-CF composite's wear surface experienced tribo-chemical reactions, and three kinds of oxides (including TiO_2 , SiO_2 and CaO) were generated. Then, the frictional heat could provide enough energy to promote the continuous generation of oxides, forming an oxide layer of TSC-CF.

Moreover, the formed oxide layer exhibited obvious plastic flow, making it easier to shear. Additionally, this oxide film prevented direct contact between TSC-CF and Inconel 718 alloy, and reduced shedding of Ti_3SiC_2 grains and material transfer. Therefore, TSC-CF showed little friction behavior.

An interesting phenomenon in this study was the oxidation of Si in the friction layer. At 25 °C, the formation rate of SiO_2 was lower than its consumption rate. The detection of silicon oxide on the wear surface of TSC-CF was irrefutable evidence of the occurrence of tribochemical reactions. However, the TSC-CF wear surface did not form an oxide layer at 25 °C, so it exhibited a high friction coefficient. At 800 °C, complete tribochemical reactions occurred and a large area of plastic flow appeared on the friction surface of TSC-CF. The elevated temperature facilitated the maintenance of the oxide layer on the friction surface. This oxide layer prevented the direct contact between TSC-CF and Inconel 718 alloy, reducing the shedding of Ti_3SiC_2 grains and material transfer. The oxide layer on the TSC-CF friction surface showed significant plastic flow and it was easier to shear. Furthermore, its brittle fracture was obviously reduced. All these factors made TSC-CF reduce friction and have high wear resistance.

5. Conclusions

The tribological behavior of the $\text{Ti}_3\text{SiC}_2/\text{CaF}_2$ -Inconel 718 tribo-pair strongly depends on the environmental temperature. Differences in temperature cause changes in friction oxides. Tribo-oxidation reactions mainly included the oxidation of Ti, Si and Ca. At 25 °C, only TiO_2 and CaO were formed. At 600 °C and above, the tribo-oxidation products included TiO_2 , SiO_2 and CaO . Therefore, $\text{Ti}_3\text{SiC}_2/\text{CaF}_2$ exhibited better self-lubricating properties than Ti_3SiC_2 at 600 and 800 °C. The addition of CaF_2 was effective at improving the self-lubricating performance of Ti_3SiC_2 at 600 and 800 °C.

Author Contributions: Conceptualization, R.Z.; Data curation, R.Z. and W.F.; Investigation, W.F.; Validation, R.Z.; Writing-original draft, R.Z.; Writing-review & editing, R.Z. and F.L. All authors have read and agreed to the published version of the manuscript.

Funding: This research received no external funding.

Institutional Review Board Statement: Not applicable.

Informed Consent Statement: Not applicable.

Data Availability Statement: The data presented in this study are available within the article.

Acknowledgments: The author acknowledges the financial support from the “Xinjiang Tianchi hundred Talents Program (Zhang Rui)”.

Conflicts of Interest: The authors declare no conflict of interest.

References

1. Barsoum, M.W.; El-Raghy, T. Synthesis and Characterization of a Remarkable Ceramic: Ti_3SiC_2 . *J. Am. Ceram. Soc.* **1996**, *79*, 1953–1956. [[CrossRef](#)]
2. Barsoum, M.W. The $M_{n+1}AX_n$ phases: A new class of solids: Thermodynamically stable nanolaminates. *Prog. Solid State Chem.* **2000**, *28*, 201–281. [[CrossRef](#)]
3. Barsoum, M.; El-Raghy, T.; Radovic, M. High-performance ceramics Ti_3SiC_2 : A layered machinable ductile carbide. *Interceram* **2000**, *49*, 226–233.
4. Gupta, S.; Barsoum, M. On the tribology of the MAX phases and their composites during dry sliding: A review. *Wear* **2011**, *271*, 1878–1894. [[CrossRef](#)]
5. Braic, M.; Balaceanu, M.; Parau, A.C.; Dinu, M.; Vladescu, A. Investigation of multilayered TiSiC/NiC protective coatings. *Vacuum* **2015**, *120*, 60–66. [[CrossRef](#)]
6. Chen, H.; Peng, J.; Fu, L. Effects of interfacial reaction and atomic diffusion on the mechanical property of Ti_3SiC_2 ceramic to Cu brazing joints. *Vacuum* **2016**, *130*, 56–62. [[CrossRef](#)]
7. Vishnyakov, V.; Lu, J.; Eklund, P.; Hultman, L.; Colligon, J. Ti_3SiC_2 -formation during Ti–C–Si multilayer deposition by magnetron sputtering at 650 °C. *Vacuum* **2013**, *93*, 56–59. [[CrossRef](#)]
8. Sarkar, D.; Basu, B.; Cho, S.J.; Chu, M.C.; Hwang, S.S.; Park, S.W. Tribological Properties of Ti_3SiC_2 . *J. Am. Ceram. Soc.* **2005**, *88*, 3245–3248. [[CrossRef](#)]

9. Ren, S.; Meng, J.; Wang, J.; Lu, J.; Yang, S. Friction and Wear of Thermal Oxidation-Treated Ti_3SiC_2 . *Tribol. Lett.* **2009**, *37*, 59–67. [[CrossRef](#)]
10. Gupta, S.; Filimonov, D.; Palanisamy, T.; Barsoum, M. Tribological behavior of select MAX phases against Al_2O_3 at elevated temperatures. *Wear* **2008**, *265*, 560–565. [[CrossRef](#)]
11. Wang, X.Y.; Shi, G.P.; Li, Q.G.; Wu, J.Y.; Wu, H.; Zhang, L.; Wang, Z. Effect of Ge on microstructure and mechanical properties of Ti_3SiC_2/Al_2O_3 composites. *Ceram. Int.* **2021**, *47*, 2280–2287. [[CrossRef](#)]
12. Hou, Q.; Yin, H.-F.; Yuan, H.-D.; Tang, Y.; Cai, Y.-Z. Fabrication of TiO_2 Nanostructures on Ti_3SiC_2 Substrate by Anodic Oxidation. *J. Nanosci. Nanotechnol.* **2018**, *18*, 1983–1988. [[CrossRef](#)] [[PubMed](#)]
13. Yin, X.; Chen, K.X.; Zhou, H.P.; Ning, X.S. Combustion Synthesis of Ti_3SiC_2/TiC Composites from Elemental Powders under High-Gravity Conditions. *J. Am. Ceram. Soc.* **2010**, *93*, 2182–2187. [[CrossRef](#)]
14. Yin, X.H.; Li, M.S.; Zhou, Y.C. Microstructure and mechanical strength of diffusion-bonded Ti_3SiC_2/Ni joints. *J. Mater. Res.* **2006**, *21*, 2415–2421. [[CrossRef](#)]
15. Wang, Q.; Chen, G.-Q.; Wang, K.; Fu, X.-S.; Zhou, W.-L. Effects of doping Ti_3SiC_2 with Al on interfacial microstructural evolution, growth kinetics and mechanical properties of $Ti_3SiC_2/TiAl$ joints. *J. Mater. Res. Technol.* **2020**, *9*, 13206–13215. [[CrossRef](#)]
16. Sonoda, T.; Nakao, S.; Ikeyama, M. Deposition and characterization of MAX-phase containing Ti–Si–C thin films by sputtering using elemental targets. *Vacuum* **2013**, *92*, 95–99. [[CrossRef](#)]
17. Ahmadifard, S.; Momeni, A.; Bahmanzadeh, S.; Kazemi, S. Microstructure, tribological and mechanical properties of $Al7075/Ti_3AlC_2$ MAX-phase surface composite produced by friction stir processing. *Vacuum* **2018**, *155*, 134–141. [[CrossRef](#)]
18. Luo, B.; Zhou, H.; Liu, D.; Luo, F.; Tian, Y.; Chen, D.; Wei, W. One-step in-situ reaction synthesis of TiC/graphene composite thin film for titanium foil surface reinforcement. *Vacuum* **2019**, *160*, 472–477. [[CrossRef](#)]
19. Lisitsyn, V.M.; Lisitsyna, L.A.; Popov, A.I.; Kotomin, E.A.; Abuova, F.U.; Akilbekov, A.; Maier, J. Stabilization of primary mobile radiation defects in MgF_2 crystals. *Nucl. Instrum. Methods Phys. Res. Sect. B* **2016**, *374*, 24–28. [[CrossRef](#)]
20. Kotomin, E.A. Nuclear Instruments and Methods in Physics Research section B: Beam interactions with materials and atoms. *Nucl. Instrum. Methods Phys. Res. Sect. B* **2022**, *511*, 17. [[CrossRef](#)]
21. Ochs, D.; Brause, M.; Krischok, S.; Stracke, P.; Maus-Friedrichs, W.; Puchin, V.; Popov, A.; Kempter, V. Characterization of LiF and CaF_2 surfaces using MIES and UPS (HeI). *J. Electron Spectrosc. Relat. Phenom.* **1998**, *88–91*, 725–732. [[CrossRef](#)]
22. Zhu, S.; Bi, Q.; Yang, J.; Liu, W. Effect of Fluoride Content on Friction and Wear Performance of Ni_3Al Matrix High-Temperature Self-Lubricating Composites. *Tribol. Lett.* **2011**, *43*, 341–349. [[CrossRef](#)]
23. Benamor, A.; Hadji, Y.; Chiker, N.; Haddad, A.; Guedouar, B.; Labaiz, M.; Hakem, M.; Tricoteaux, A.; Nivot, C.; Erauw, J.P.; et al. Spark Plasma Sintering and tribological behavior of $Ti_3SiC_2-Ti_5Si_3-TiC$ composites. *Ceram. Int.* **2019**, *45*, 21781–21792. [[CrossRef](#)]
24. Ouyang, J.H.; Sasaki, S.; Murakami, T.; Umeda, K. The synergistic effects of CaF_2 and Au lubricants on tribological properties of spark-plasma-sintered $ZrO_2(Y_2O_3)$ matrix composites. *Mat. Sci. Eng. A* **2004**, *386*, 234–243. [[CrossRef](#)]
25. Ouyang, J.; Sasaki, S.; Murakami, T.; Umeda, K. Tribological properties of spark-plasma-sintered $ZrO_2(Y_2O_3)-CaF_2-Ag$ composites at elevated temperatures. *Wear* **2005**, *258*, 1444–1454. [[CrossRef](#)]
26. Zhang, R.; Feng, K.; Meng, J.; Su, B.; Ren, S.; Hai, W. Synthesis and characterization of spark plasma sintered Ti_3SiC_2/Pb composites. *Ceram. Int.* **2015**, *41*, 10380–10386. [[CrossRef](#)]
27. Wu, E.; Kisi, E.H.; Kennedy, S.J.; Studer, A.J. In Situ Neutron Powder Diffraction Study of Ti_3SiC_2 Synthesis. *J. Am. Ceram. Soc.* **2004**, *84*, 2281–2288. [[CrossRef](#)]
28. Huang, Z.; Zhai, H.; Guan, M.; Liu, X.; Ai, M.; Zhou, Y. Oxide-film-dependent tribological behaviors of Ti_3SiC_2 . *Wear* **2007**, *262*, 1079–1085. [[CrossRef](#)]